Blending of Series-Parallel Compliant Actuation With Field Weakening Control for Explosive Motion Generation

Vishnu Dev Amara, Jörn Malzahn, Wesley Roozing, and Nikos Tsagarakis

***Abstract*—In this work, we investigate and validate two methods that can extend the explosive motion capabilities of series elastic actuated robots during standing jumps. First, field weakening control is exploited on multiple joints of a monoped to boost their peak velocities. However, field weakening operation reduces actuation torque capacity at those velocities, due to consuming current reserves. To address this torque reduction, we leverage energy-efficient parallel elastic actuators, in biarticulated knee-ankle and monoarticulated knee configuration. The proposed concept therefore combines the torque and inter-joint power transfer benefits of parallel and biarticulated articulation with the velocity increase permitted by field weakening to amplify the explosive power output in a monoped robot prototype. A substantial performance increase of up to 54% in jump height is achieved after experimentally tuning the motion for each configuration. This validates the efficacy of the approach for improving the explosive capabilities of series elastic actuated robots.**

***Index Terms*—Legged robots, motion control, humanoid and bipedal locomotion, soft sensors and actuators.**

I. Introduction

IN THE immediate aftermath of calamities, versatile legged robots are expected to potentially intervene and aid humans in rescue efforts. Legged robots have to be agile in cluttered environments and require long periods of autonomous operation. Many high-performance legged robots such as CENTAURO [1] and Valkyrie [2] are driven by series-elastic actuation (SEA). SEAs supported by high ratio gearboxes offer high torque capacity and power density, accurate torque control, as well as the ability to sustain shock impacts. This makes them ideal for operation in unstructured environments.

Explosive human motions involve peak joint velocities that can exceed 50 rad/s [3]. Highly dynamic motions including jumping, hopping and throwing are accomplished through features including parallel muscle mechanisms, inter-joint power transfer through biarticulation [4], and energy storage and release capabilities [5] in their musculo-skeletal system. Many biomechanical studies [4], [6], [7] also suggest the notable role of ankle aided by biarticulation in dynamic locomotion tasks. In general, biarticular muscles that span two joints serve a unique role of power transfer from proximal to distal joints in several ballistic tasks permitting biological systems to demonstrate highly dynamic motion skills.

However, the peak velocities of high torque, high power SEAs are limited by their high transmission ratios and voltage limits. Therefore it is only natural to envision intrinsically SEA powered robots augmented with biomimetic actuation principles such as biarticulation [8] and parallel compliance [9] to improve both energy-efficiency and peak performance. Previous works on the use of multi-articulated parallel elastic actuation (PEA) on an anthropomorphic robotic limb powered by SEAs demonstrated substantial energy savings during periodic squat motions [10], [11]. Although the energy efficiency characteristics of PEAs have been amply addressed, their benefit in improving the peak power characteristics of robotic systems has not been thoroughly explored.

Approaches to maximize the link velocity in SEA joints are fairly limited to exciting the spring element so as to amplify link velocities higher than the motor velocities [12], [13]. At the same time, a well-established method called field weakening (FW) control [14] is commonly used to boost the speed of industrial drives with voltage constraints. Yet, this technique has not been significantly explored in robotics. FW draws on the electrical motor dynamics to decrease the back-EMF and subsequently the voltage requirements for a given velocity, therefore higher velocities can be attained with the same supply voltage constraints. Recently, FW was employed in [15], with promising results showing up to 33% increased peak velocity in series elastic actuation drives.

Motivated by the above principles and methods, in this work we propose a novel approach that pairs FW control with principles of parallel articulation and inter-joint power transfer to further enhance dynamic performance and demonstrate this in explosive jumping tasks executed by a monoped robot prototype. Contrary to existing works which feature either an active or passive biarticular spring to aid ankle extension during running [8], jumping [16] or leaping [17] tasks, the monoped prototype used

Manuscript received October 15, 2020; accepted January 28, 2021. Date of publication February 22, 2021; date of current version March 10, 2021. This letter was recommended for publication by Associate Editor C.-H. Kuo and Editor C. Gosselin upon evaluation of the reviewers' comments. This work was supported by the IIT internal funding. *(Corresponding author: Vishnu Dev Amara.)*

Vishnu Dev Amara, Jörn Malzahn, and Nikos Tsagarakis are with the Humanoids and Human-Centered Mechatronics Lab, Istituto Italiano di Tecnologia (IIT), Genova 16163, Italy (e-mail: vishnu.amara@iit.it; jorn.malzahn@iit.it; nikos.tsagarakis@iit.it).

Wesley Roozing is with the Department of Robotics and Mechatronics (RAM), University of Twente, Enschede 7522NB, The Netherlands (e-mail: w.roozing@utwente.nl).

This letter has supplementary downloadable material available at https://doi.org/10.1109/LRA.2021.3061066, provided by the authors.

Digital Object Identifier 10.1109/LRA.2021.3061066

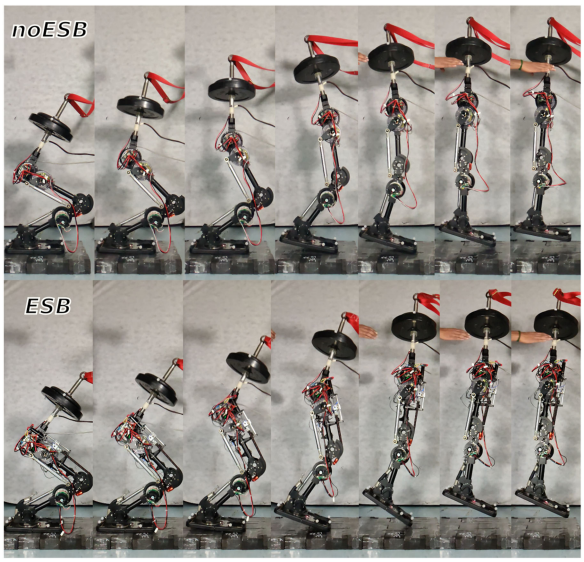

Fig. 1. Snapshots of jump experiments with *noESB* (above) and *ESB* (below) configurations. Notice the visible difference in foot height at apex.

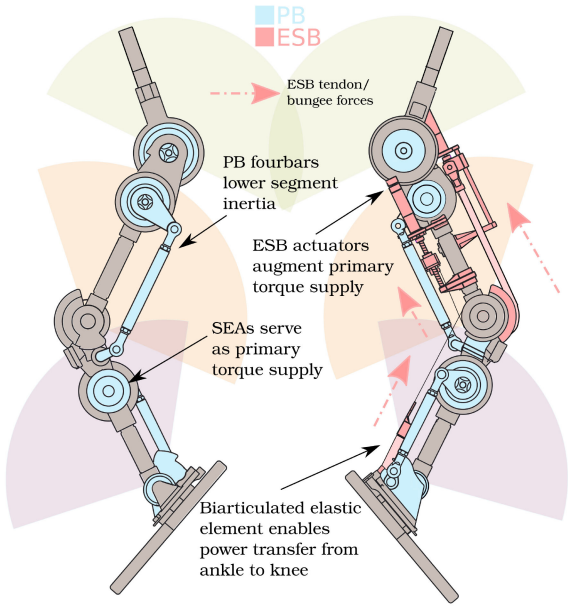

Fig. 2. Schematics of the *noESB* and *ESB* configurations of eLeg. The tinted areas indicate the ranges of joint motion.

in this work employs in addition, a monoarticulated parallel actuator to aid knee extension. Compared to [18], [19] which feature active monoarticular and/or biarticular parallel actuators alone, we additionally utilize SEAs.

- demonstrate FW control on a multi-link SEA-driven monoped robot called eLeg [10], [20] to perform standing jumps (Fig. 1),
- validate and discuss why by applying FW alone may not enhance the explosive motion sufficiently and
- pair FW technique with energy-efficient parallel articulation and biarticulation principles, to substantially increase the explosive motion performance of a monoped robot prototype.

To the best of our knowledge, this is the first experimental demonstration of FW on a multi-link torque controlled robot.

The letter is organized as follows. Sections II and III provide a brief overview on the hardware prototype and field weakening controller. The jump controller is presented in Section IV and the experimental results are discussed in Section V. The letter finally concludes in Section VII.

II. Multi-Articulated Compliant Eleg

The testbed that we utilize in this letter is eLeg [21], shown in Fig. 2. It is a three degrees of freedom (DoF), floating-base, planar leg prototype that stands about 1 m tall and is actuated by SEAs referred to as the Power Branches (PB). In addition, it also permits to employ parallel compliant actuation arrangements (ACA). These comprise high energy-capacity, low stiffness, parallel compliant elements called the Energy Storage Branch (ESB). The ESBs are driven by low power, highly-efficient DC motors with high gear ratios. Stretchable bungee cords that display unidirectional force characteristics serve as parallel compliant tendons that can store large amounts of potential energy.

The modular parallel elements can be reconfigured into mono- and biarticulated actuation topologies. When in biarticulation, the ESB element applies torques to both the spanned joints as well as allow for power transfer between them. The full details of eLeg design and hardware can be found in [20]. The PB torques are measured by torque sensors present in the SEAs and bungee forces are measured by strain gauges at the ESB actuators.

Given an $n+3$ DoF planar floating-base robot with m ($\leq n$) ACA branches, the ESB forces can be resolved into joint torques based on the articulation topology [10]:

$$\boldsymbol{\tau}_{\mathbf{p}} = -\mathbf{T}^{\mathbf{T}}\,\mathbf{F}_{\mathbf{p}} = -\mathbf{T}^{\mathbf{T}}\mathbf{K}(\mathbf{S}\mathbf{p}+\mathbf{T}\mathbf{q}), \tag{1}$$

where $\boldsymbol{\tau}_p$ is the component of joint torque from the parallel elements. $\mathbf{T} \in \mathbb{R}^{n\times n}$ is a topology matrix that is a function of tendon transmission ratio and ESB arrangements. $\mathbf{S} \in \mathbb{R}^{n\times m}$ is a selection matrix that chooses the joints which comprise ESB elements. $\mathbf{q} \in \mathbb{R}^n$ denotes the joint configuration that correspond to the actuated DoFs and $\mathbf{p} \in \mathbb{R}^m$ denotes the tendon pretensions, $\mathbf{F}_{\mathbf{p}} \in \mathbb{R}^m$ denotes the unilateral tendon forces. Thus, net torques at the joints are,

$$\boldsymbol{\tau} = \boldsymbol{\tau}_{PB} + \boldsymbol{\tau}_p\,. \tag{2}$$

The hip joint is loaded with a 15 kg dead-weight simulating the trunk. This work employs two distinct configurations:

i) **noESB**: all joints are only powered by the SEAs in PBs. The robot weighs 26.6 kg in this configuration.
ii) **ESB**: in addition to PBs, two ESBs are added. The ankle ESB is biarticulated and spans both ankle and knee and the knee ESB is monoarticulated. The robot weighs 28 kg in this configuration with the ESBs added.

III. Field Weakening for SEAs

The steady-state voltage equations for a Surface Permanent Magnet Synchronous Motor[1] (SPMSM) [23] are,

$$\begin{aligned} v_d &= R\, i_d \;-\; n_p\, N\, L\, i_q\, \dot{\theta}, \\ v_q &= R\, i_q \;+\; n_p\, N\, L\, i_d\, \dot{\theta} \;+\; \underbrace{n_p\, N\, \psi\, \dot{\theta}}_{\text{back-EMF}}, \end{aligned} \tag{3}$$

subject to the operating constraints:

$$v_d^2 \;+\; v_q^2 \;\leq\; v_{\max}^2, \quad i_d^2 \;+\; i_q^2 \;\leq\; i_{\max}^2 \tag{4}$$

where v_d, v_q, i_d and i_q denote the direct and quadrature voltages and currents respectively. L is the inductance along both the current axes (for SPMSM, $L_d = L_q = L$), ψ is the flux linkage of the motor, n_p is the number of poles in the motor and R is its electrical winding resistance. $\dot{\theta}$ and N are the gear output velocity and gear ratio of the particular SEA. $v_{\max}$ and $i_{\max}$ are the maximum inverter phase-voltage and phase-current. The SEA electromotive torque can be related to the quadrature current as,

$$\tau_m = \frac{3}{2}\, n_p\, \psi\, N\, i_q. \tag{5}$$

Application of any non-zero direct current i_d does not result in usable work at the gear output for SPMSM. Therefore, conventional motor operation relies on the Maximum Torque per Ampere (MTPA) strategy where the magnitude of direct current is generally zero. In (3), back-EMF increases quadrature voltage with increasing velocity, leading to limited velocity for a certain level of supply voltage. By leveraging the quadrature voltage created by direct current, current reserves can be utilised to attain higher velocities within the operating constraints (4). Assuming $\dot{\theta} \geq 0$, the quadrature voltage can be reduced by a negative direct current. However, this also results in reducing the torque generating quadrature current due to the current limit in (4). In other words, FW allows to avoid voltage saturation for higher velocities but at the expense of torque capacity.

To realize FW, we adopt the state-less inverse electrical dynamics controller presented in [15], the action of which is schematically visualized on $i_q - \dot{\theta}$ plane in Fig. 3 for the frictionless case. The FW controller generates current references in the d-q plane according to desired torque and current velocity, from zero torque at point O to A (MTPA, mode 0) through A to B (voltage saturated phase, mode 1) and B to max field weakened velocity, C (current saturated phase, mode 2).

Finally, although the theoretical maximum attainable FW speed is quite high for the frictionless joint, in practice, this value is reduced due to motor and gearbox friction, inertial effects and external forces. The electrical parameters of the motors utilized in this work can be found in [15].

IV. Jump Controller

Fig. 4 shows the control architecture adopted in this work. Jumping motion plans for both configurations of the robot are

[1]Motors in the Alberobotics Orange SEAs [22] used here are SPMSMs.

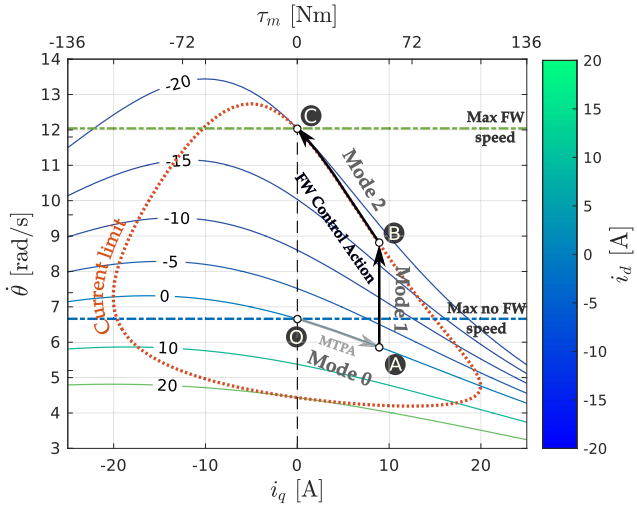

Fig. 3. FW controller schematic on the upper half of $i_q - \dot{\theta}$ plane. The blue-green solid isolines indicate voltage limit curves for various i_d currents. The current limit is depicted by red locus. The dash-dotted horizontal lines indicate the maximum no-FW speed (blue) and maximum FW speed (green) at the gear output, in the frictionless case. Black arrows indicate directions along which the current references are generated by the controller. The electromotive torque corresponding to i_q is plotted on x-axis above. While field-weakening enhances the y-intercept (velocity), PEAs can augment the loss in torque due to reduction of the x-intercept (electromotive torque).

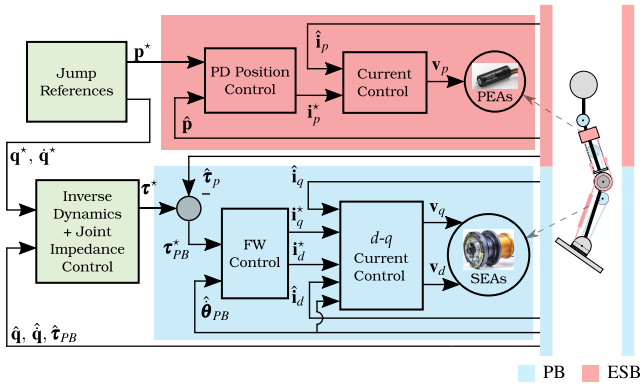

Fig. 4. Schematic of the controller used in this work. $(\hat{\cdot})$ and $(\cdot^\star)$ refer to measured and reference signals.

obtained by tuning for position trajectories of the ankle, knee and hip joints to facilitate rapid leg extensions. Accordingly, we parameterize the second order continuous (C^2-continuous) joint reference trajectories for both *noESB* and *ESB* configurations with the duration of extension motion, their initial and final joint angles. Given the joint configuration limits, we set the initial pose of the robot such that its center of mass (CoM) is at the lowest possible point while keeping the center of pressure (CoP) within the foot. This is done to maximize available range of motion at the joints. The final configuration of the robot at the moment of take-off is tuned based on heuristics such as a near-singularity robot pose and an extended ankle configuration. The extension duration is limited to less than 0.5 s for both configurations. In this way, position and velocity references are experimentally tuned to obtain the highest possible vertical CoM displacement for both *noESB* and *ESB* configurations, see Fig. 5.

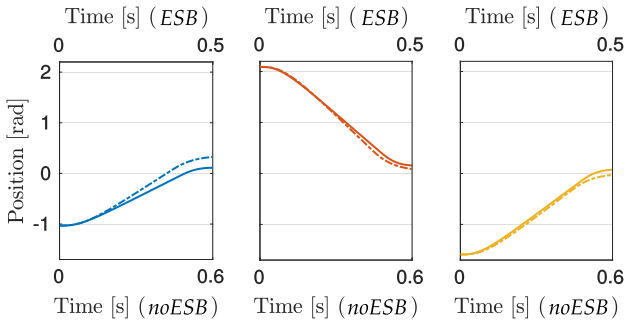

Fig. 5. The motion references used for the *noESB* (solid) and *ESB* (dash-dotted) configurations for ankle (blue), knee (red) and hip (yellow) joints until about the apex are shown.

We use an inverse dynamics controller with a PD joint impedance loop to generate the joint torque references. Given the lack of ground constraint force estimates, we neglect the constraint force terms in the inverse dynamics controller:

$$\boldsymbol{\tau}^{\star} = \mathbf{H}(\mathbf{q})\,\ddot{\mathbf{q}}^{\star} + \mathbf{c}(\mathbf{q},\dot{\mathbf{q}}) + \mathbf{K}_p(\mathbf{q}^{\star}-\mathbf{q}) + \mathbf{K}_d(\dot{\mathbf{q}}^{\star}-\dot{\mathbf{q}}), \tag{6}$$

where $\mathbf{H}$ and $\mathbf{c}$ comprise the rows of the joint-space inertia matrix and joint space bias forces (Coriolis, damping and gravity torques) that correspond to the actuated DoFs. We use diagonal impedance gain matrices, $\mathbf{K}_p = \text{diag}([1500,\ 1600,\ 1200])$ Nm/rad and $\mathbf{K}_d = \text{diag}([12,\ 13,\ 10])$ Nms/rad.

For the ESB (shown in red), a cascaded controller with 1 kHz outer PD position control loop and an inner 20 kHz MTPA based PI current control loop is employed. We experimentally tuned the pretensions to 14 mm and 45 mm for the biarticular and monoarticular ESBs for all the *ESB* configuration jumps. Although the ESBs can be actively controlled, their maximum translational velocities are lower than 8 mm/s. Due to sub-second jump duration, the maximum change in bungee pretensions is limited to 4 mm. Hence, we maintain constant pretensions during the jumps.

For the PB (shown in blue), we adopt a multi-rate cascaded controller. PB torque references are computed by subtracting the ESB tendon contributions from the joint torque references. Subsequently, the FW controller converts them to current references in the d-q plane at 1 kHz following the strategy described in Section III. In the absence of FW, the torque references are directly converted to quadrature current references. Two inner d-q current control loops that comprise feedforward, back-EMF, cross-coupling and PI terms are utilized for the current control, see (3). While, torque and current references are generated from Simulink-RealTime at 1 kHz, current control is executed in the embedded DSP boards of the actuator drivers at 20 kHz. A current limit of 20 A ($\sim$124 Nm) is applied on all SEAs across experiments.

Instantaneous electrical and mechanical joint powers can be computed as,

$$\mathbf{P}_e = \underbrace{\frac{3}{2}(\mathbf{v}_q^T\ \mathbf{i}_q + \mathbf{v}_d^T\ \mathbf{i}_d)}_{\text{PB}} + \underbrace{\mathbf{v}_p^T\,\mathbf{i}_p}_{\text{ESB}}, \tag{7}$$

$$\mathbf{P}_m = \underbrace{\boldsymbol{\tau}_{PB}^T\,\dot{\mathbf{q}}}_{\text{PB}} + \underbrace{(-\mathbf{F}_p^T\,\mathbf{T}\dot{\mathbf{q}})}_{\text{ESB}}, \tag{8}$$

where the voltages are computed using (3) with current measurements from sensors on the embedded electronics.

Since the robot lacks real-time estimation of foot position and orientation in the world frame, we do not employ any sophisticated landing controller. Jump motion references are tuned for the two configurations such that when they are applied on the corresponding configuration, the angular momentum of the robot at the apex is not significant.

V. Experiments

The jump experiments are executed on an Intel NUC PC with 2 GB DDR-3 RAM and a 1.8 GHz Core i5-3427 U processor. We rate the explosive motion by measuring the vertical CoM displacement of eLeg, from its stance position (singular configuration) to its apex during the jump. We alternatively refer to the CoM displacement at apex from stance as *jump height* in this letter. The hip joint does not require substantial torques as compared to the other joints during the explosive motion, which prevents the onset of voltage saturated phase and the triggering of the FW for that joint. In addition, the ankle and knee joints are the major contributors to vertical CoM velocity and augmented with ESBs. Thus, we present experimental details only for the ankle and knee joints.

A. Jumps Tuned for noESB Configuration

Fig. 6 shows results of experiments where joint references are tuned for the *noESB* configuration to maximize vertical CoM displacement. Measured SEA currents are filtered with a 200 Hz low-pass filter. Data is shown from start of the jumping motion to the instant the CoM reaches apex height. Fig. 7 summarises numerical details including CoM and foot displacements, vertical take-off velocity at take-off, peak joint velocities and torques, average mechanical and electrical powers.

1) Jump #1: In the left column of Fig. 6, in the absence of FW, from the SEA d-q current tracking plots, while direct currents are minimized, the quadrature current tracking quality worsens as the jump motion progresses. This is due to voltage saturation that occurs at high velocities. It is also visible that the peak joint velocities are all below 6.6 rad/s (maximum no FW speed, see Fig. 3). From the torque plots, it is clear that as the robot extends and approaches singularity, the torque output reduces. The power plots indicate that initially the knee is the major contributor to increasing vertical CoM velocity, until approaching full extension, at which point the ankle takes over. The achieved CoM displacement from stance pose is 9.6 cm.

2) Jump #2: In the middle column of Fig. 6, we show data for the same joint references with FW enabled on the *noESB* configuration. The d-q SEA current plots indicate the action of FW controller - the joints avoids voltage saturation maintaining good tracking quality. The knee current reference tracking suffers slightly at the end, potentially due to variation of electrical parameters from estimated values used in the current controller. The resulting CoM displacement from stance is 11 cm, a 15%

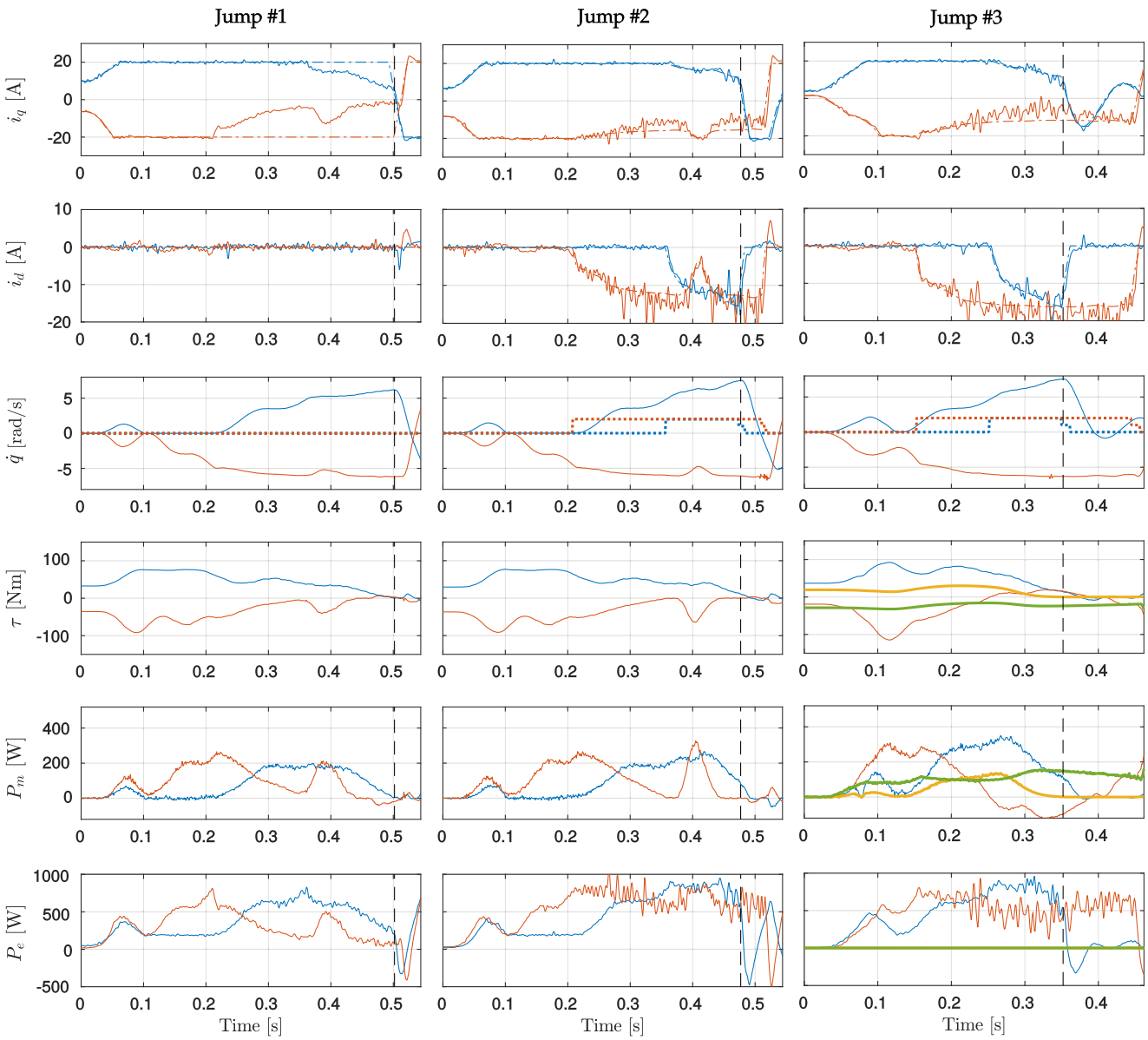

Fig. 6. Data from jumps tuned for *noESB* configuration, for **ankle** (blue) and **knee** (red): left column (*noESB*, **no FW**, **jump** #**1**), middle column (*noESB*, **with FW**, **jump** #**2**) and right column (*ESB*, **with FW**, **jump** #**3**), dash-dotted lines (references), solid lines (measured). SEA d-q current tracking, resulting joint velocities, torques, mechanical and electrical powers are shown. Torques and powers corresponding to ankle-knee biarticular ESB and knee monoarticular ESB are shown with yellow and green solid lines respectively. Dotted lines indicate FW modes. Vertical dashed lines indicate take-off moments. CoM stance displacement: **9.60 cm** (*noESB*), **11.01 cm** (*noESB* **with FW**) and **13.17 cm** (*ESB* **with FW**).

increase over without FW. While FW increases peak velocities, the ankle remains stationary during the initial part of the motion (between 0.1 to 0.2 s), as seen in the velocity plot (also refer to jump #2 in video attachment). Although, the SEA quadrature current is saturated, there is a shortage of torque at those instants at the the ankle. This observation asserts that the ankle can potentially benefit from additional torques from PEAs and lead to improved jump motions.

3) Jump #3: We apply the same joint motion references tuned for the *noESB* configuration to the *ESB* configuration with FW enabled. Fig. 6 illustrates the corresponding data in the right column. The plots of the SEA currents indicate that the tracked quadrature currents are noticeably smaller than jump #2 (*noESB* with FW). Yet, the peak torques are higher as reported in table in Fig. 7. This is due to the joint torques augmented by the ESBs. Moreover, the additional ESB torques also lead to quicker velocity build-up as compared with jump #2. Increase in peak velocity at knee (6.6 rad/s) is limited when compared to the ankle (7.5 rad/s). Notice how the net joint torque at the knee changes sign and becomes positive although both the torque-generating quadrature current at SEA as well as its reference are negative. Although the knee joint approaches its peak velocity quite early, it remains at the same level throughout. This phenomenon can be attributed to the influx of power from the multi-body robot dynamics and biarticular power transfer from knee to ankle throughout the jump. The latter is exemplified in [16], where timely activation/deactivation of the biarticular spring can help prevent this undesired effect. In eLeg, the

Specification	tuned for *noESB*			tuned for *ESB*	
	noESB #1	*noESB*, FW #2	*ESB*, FW #3	*noESB* #4	*ESB*, FW #5
CoM stance displacement (cm)	**9.60**	**11.01**	**13.17**	**2.62**	**14.78**
CoM squat displacement (cm)	39.03	40.47	42.98	32.48	45.01
Foot CoM displacement (cm)	8.36	10.05	13.22	11.19	15.00
CoM take-off velocity (m/s)	1.12	1.31	1.54	0.86	1.60
Peak ankle velocity (rad/s)	6.20	7.53	7.56	6.26	7.79
Peak knee velocity (rad/s)	-6.24	-6.71	-6.63	-6.24	-6.74
Peak ankle torque (Nm)	76.58	77.81	92.60	76.84	92.79
Peak knee torque (Nm)	-91.80	-91.26	-114.66	-94.66	-126.17
Average mechanical power output (W)	185.49	200.16	228.86	188.52	238.10
Average electrical power consumed (W)	694.00	993.02	899.15	684.47	947.16

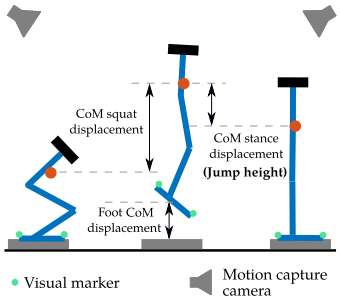

Fig. 7. Numerical details from all experiments reported in the letter along with a visual description of the various measured CoM displacements. Indicated displacements and velocity are computed for the vertical direction. Reported powers are computed as the averages of the sum of ankle and knee powers until the moment of take-off. Red dot indicates CoM of the monoped. *Jump height* is measured as CoM stance displacement.

unilateral ESB tendon forces cannot be activated/deactivated at will during mid-motion. Nonetheless, owing to the ESB tendons, the mechanical power output from the two joints are higher than the *noESB* case leading to a jump height of 13.2 cm, 37% higher than jump #1. Furthermore, given the presence of biarticular ESB, which enables power transfer from knee to ankle, the contribution of ankle power to the heel push-off and hence the jump motion performance is substantially increased.

B. *Jumps Tuned for* ESB *Configuration*

The *ESB* configuration in jump #3 brought about a marked enhancement over the *noESB* configuration. However, mass and inertia distribution across the various links in the *ESB* configuration differs from the *noESB* configuration. Due to these differences as well as additional PEAs, we investigate if joint motion references specifically tuned for the *ESB* configuration can further enhance jumping performance. The corresponding results in the presence of FW (jump #5) are reported in the right column of Fig. 8. Since the reported experiments involve hand tuning, to establish a fair comparison, we apply the same joint motion reference trajectories on the *noESB* configuration as well (jump #4), shown in the left column of Fig. 8. Additional numerical details are displayed in Fig. 7.

1) Jump #4: From jump #4, it becomes immediately clear that the references suitable for the *ESB* configuration are not suitable for *noESB* configuration, since the robot CoM pitches too much forward owing to significant angular momentum from the extension motion (refer to the video attachment). Although joint velocities exceed 6 rad/s and joint torques and mechanical power profiles are similar to the previous *noESB* jump, the corresponding CoM vertical displacement from a stance pose is only about 2.6 cm, significantly worse than jump #1. Moreover, the robot does not land safely after the jump (not shown).

2) Jump #5: As for the *ESB*-tuned motions on the *ESB* configuration (jump #5), depicted in Fig. 8, the PEAs supply part of the joint torques and hence allow to lower torque generating quadrature current references for SEAs. As a result, higher current reserves are available to be leveraged by the FW controller. Consequently, the joints achieve the highest velocities and torques with this particular jump, among all the jumps reported in this work (as shown in the table in Fig. 7). We ascribe these observations to the motion references being specifically tuned for the *ESB* configuration. The ensuing CoM stance displacement is 14.8 cm, an increase of 54% over the *noESB*, no FW case (jump #1).

VI. Discussion

A. *Results*

1) FW With PEAs Enhance Explosive Motion Performance: Utilizing FW with trajectory tracking in torque controlled actuators is in general, non-trivial. The reference trajectories and hence the torques and currents need to saturate the voltage for FW modes to engage. This particular requirement makes it well-suited for explosive motion tasks. Accordingly, we demonstrate squat jumps through multi-DoF field weakening control on a monoped. In a first set of experiments with joint motion references tuned for *noESB* configuration, we observe that while FW can improve explosive motion performance (jump #2, +15%) compared to jump #1, addition of ESBs can bring about an even higher performance enhancement (jump #3, +37%). Now, it has been shown in [16], [24] that addition of ESBs or biarticular springs leads to a different optimal jump motion. Therefore, in a second set of experiments, we show that by tuning the motion references for *ESB* configuration, we further exploit its explosive motion potential (jump #5, +54%). The result also asserts that in a multi-joint robot, while FW can improve jump height by boosting peak velocities, combining FW with parallel articulation can lead to a considerably higher mechanical power output as a result of torque augmentation. This is especially useful during FW when operating at peak output as current limits limit the available PB torque.

2) FW Reduces Voltage Demand At the Expense of Energy-Efficiency: Compared to jump #1 (*noESB*, no FW), the sole application of FW in jump #2 leads to i) higher peak joint velocities by alleviating voltage constraints, as can be seen in their velocity plots of Fig. 6; ii) consequently, a sizeable increase in the average mechanical power output, as seen in the table in Fig. 7; iii) an increase in electrical power consumption owing to consuming voltage and current reserves, as shown in power plots in Fig. 6. Therefore, FW improves peak joint velocities while

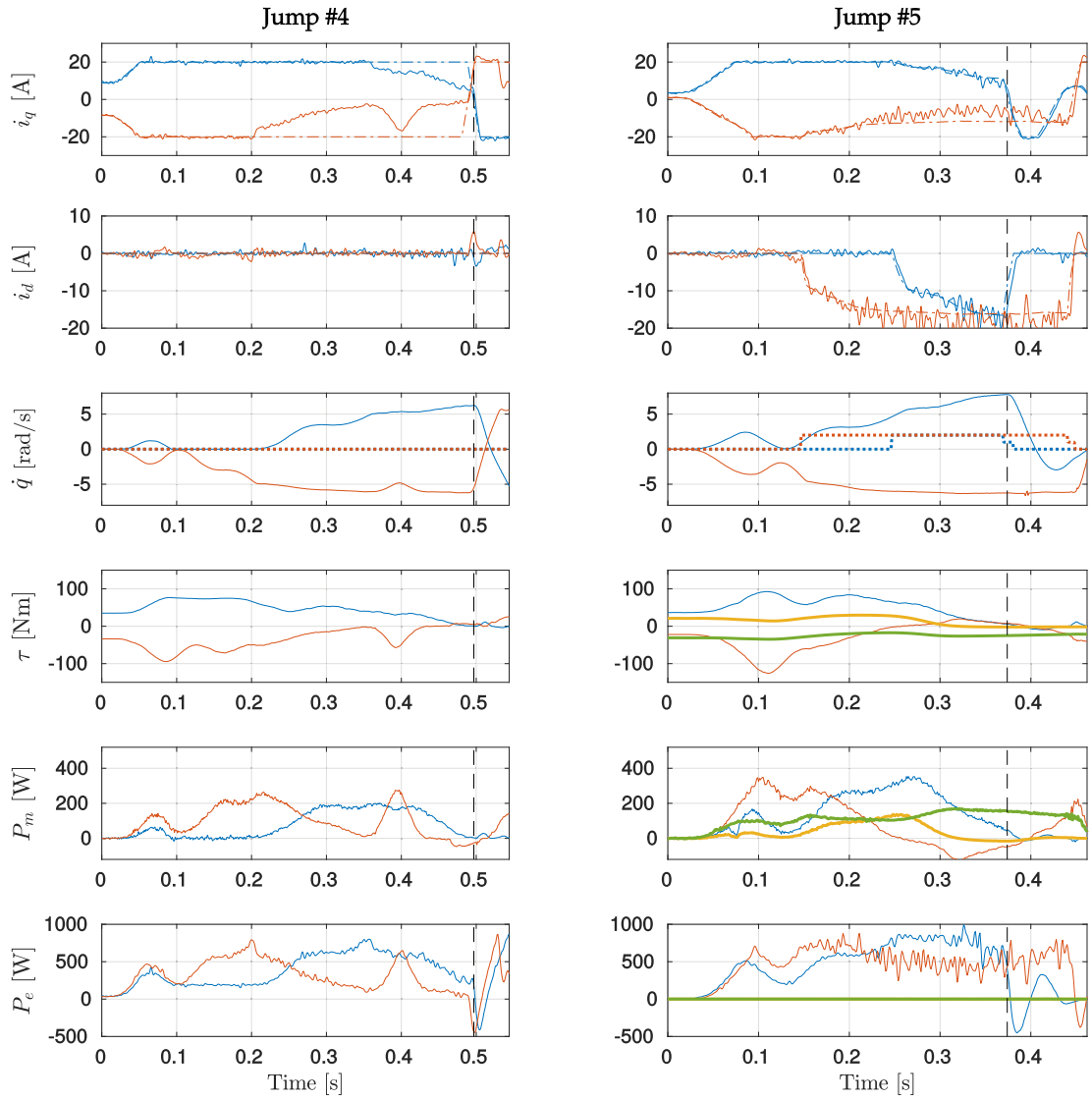

Fig. 8. Data from jumps tuned for *ESB* configuration, for **ankle** (blue) and **knee** (red): left column (*noESB* **without FW, jump #4**), right column (*ESB*, **with FW, jump #5**), dash-dotted lines (references), solid lines (measured). SEA d-q current tracking, resulting net joint velocities, net joint torques, net joint mechanical and electrical powers are shown. Torques and powers corresponding to ankle-knee biarticular ESB and knee monoarticular ESB are shown with yellow and green solid lines respectively. Dotted lines in velocity plots represent FW modes. Vertical dashed lines indicate take-off moments. CoM stance displacement: **2.62 cm (jump #4)** and **14.78 cm (jump #5)**.

sacrificing energy-efficiency. However, as FW increases power consumption only momentarily during explosive motions, this is an acceptable trade-off that allows to reduce the size and weight of system's actuators, thereby making it more efficient overall.

3) PEAs Compensate for the Loss in Energy-Efficiency Due to FW: Further addition of PEAs allows for a significantly higher mechanical power output in *ESB* jumps (#3 and #5) than the *noESB* jumps (#1 and #2), see Figs. 6–8. It is also interesting to observe that the higher expulsion of mechanical power in *ESB* jumps does not lead to any higher electrical power consumption than the *noESB*, FW case (jump #2). Moreover, power transfer from the knee to ankle explains the sizeable increase in ankle power, when compared to jump #1 (*noESB*, no FW). Further, notice the negligible ESB electrical power consumption, since pretensions are held constant throughout the jump. These observations demonstrate the energy-efficiency potential of ESBs even while executing explosive motions. The efficacy of coupling PEAs with FW can thus be seen. While FW consumes electrical power to achieve higher joint velocities, PEAs at least partially compensate for the loss in torque capacity by contributing to the mechanical power through the energy stored in its elastic elements. Concurrently, due to additional PEA torques at the joints, the quadrature current required by SEAs is also reduced as a result of their reduced torque demand.

4) Optimal Motion References are Configuration-Specific: On one hand, in jump #4, where motion references tuned for *ESB* configuration are applied to *noESB* configuration, the robot tips forward and falls over. On the other hand, the *ESB*

configuration achieves the highest jump height while applying the motion references that are tuned particularly for its configuration (jump #5 compared to #3). These results confirm that distinct optimal joint motion reference exist for different actuated configurations. Motion references tuned for a particular configuration, when applied for the other configuration are either not suitable or do not exploit the full potential towards peak performance.

B. Hardware Limitations

The biarticular ESB contributes to extension of the ankle, but also leads to flexion at the knee. Conversely, the monoarticular ESB aids in knee extension. Therefore, a trade-off exists in setting the pretensions, so as to avoid any adverse effects during the extension motion at the knee joint. The experimentally applied pretension values are heuristically tuned so as to achieve the best possible trade-off. Obtaining objectively optimal pretensions is subject to future work.

The fourbar mechanisms in both ankle and knee joints exhibit a small configuration-dependent play at times, which leads to a small difference in the initial joint configuration between the *noESB* and *ESB* configurations.

C. Future Work

Given the limited range of joint motion (less than 2.1 rd, see Fig. 5) and the dynamic nature of the explosive motion, estimating the best possible outcome from the two configurations, while operating at the boundaries of actuation, is important. The difficulty in obtaining these outcomes is further compounded by nonlinearity and hysteresis in the bungees. These considerations prompt us to apply optimization concepts such as in our earlier work [24], to plan optimal vertical jump motions while taking into account constraints arising from nonlinear mechanical and electrical dynamics and contact transitions. The same along with torque and current controller improvements would serve as valuable future work.

VII. Conclusion

This work has shown that field weakening combined with parallel actuation can result in considerable improvements to the explosive motion performance of a monoped robot. We consider two distinct eLeg actuation configurations with the same starting pose and perform standing jumps. As distinct optimal take-off motions may exist due to the addition of parallel actuators, for an impartial comparison, we conduct jumps across the two configurations with joint motion references tuned for each of them. In a first set of experiments, where the jump motion is tuned for *noESB* configuration, the results indicate that combination of FW with parallel articulation can enhance the jump performance compared to what the FW alone can provide. In a second set of experiments, specifically tuned for *ESB* configuration, we show that leveraging FW and parallel actuation together with motions that exploit them, can further improve jumping performance. The results suggest several avenues for future work that may produce further performance improvements.

References

[1] N. Kashiri *et al.*, "Centauro: A. hybrid locomotion and high power resilient manipulation platform," *IEEE Robot. Automat. Lett.*, vol. 4, no. 2, pp. 1595–1602, Apr. 2019.

[2] N. Paine *et al.*, "Actuator control for the NASA-JSC valkyrie humanoid robot: A decoupled dynamics approach for torque control of series elastic robots," *J. Field Robot.*, vol. 32, no. 3, pp. 378–396, May 2015.

[3] I. Herman, *Physics of the Human Body*. Springer Science Media, 2007.

[4] G. J. van IngenSchenau, "From rotation to translation : Constraints on multi-joint motions and the unique action of biarticulated muscles," *Hum. Movement Sci.*, vol. 8, no. 1, pp. 301–337, 1989.

[5] N. T. Roach, M. Venkadesan, M. J. Rainbow, and D. E. Lieberman, "Elastic energy storage in the shoulder and the evolution of high-speed throwing," *Nature*, vol. 498, no. 7455, pp. 483–486, 2013.

[6] L. Gregoire, H. Veeger, P. Huijing, and G. van IngenSchenau, "Role of mono- and biarticular muscles in explosive movements," *Int. J. Sports Med.*, vol. 5, no. 6, pp. 301–305, Dec. 1984.

[7] R. Jacobs, M. F. Bobbert, and G. J. van IngenSchenau, "Mechanical output from individual muscles during explosive leg extensions: The role of biarticular muscles," *J. Biomech.*, vol. 29, no. 4, pp. 513–523, 1996.

[8] F. Iida, J. Rummel, and A. Seyfarth, "Bipedal walking and running with spring-like biarticular muscles," *J. Biomech.*, vol. 41, no. 3, pp. 656–667, 2008.

[9] N. G. Tsagarakis, H. Dallali, F. Negrello, W. Roozing, G. A. Medrano-Cerda, and D. G. Caldwell, "Compliant antagonistic joint tuning for gravitational load cancellation and improved efficient mobility," in *Proc. IEEE-RAS Int. Conf. Humanoid Robots.*, 2014, pp. 924–929.

[10] W. Roozing, Z. Ren, and N. G. Tsagarakis, "An efficient leg with series-parallel and biarticular compliant actuation: Design optimization, modeling, and control of the eleg," *Int. J. Robot. Res.*, 2019.

[11] V. D. Amara, J. Malzahn, Z. Ren, W. Roozing, and N. G. Tsagarakis, "On the efficient control of series-parallel compliant articulated robots," in *Proc. IEEE Int. Conf. Robot. Automat.*, 2020, pp. 385–391.

[12] S. Haddadin, M. Weis, S. Wolf, and A. Albu-Schäffer, "Optimal control for maximizing link velocity of robotic variable stiffness joints," *IFAC Proc. Volumes*, vol. 44, pp. 6863–6871, Jan. 2011.

[13] T. Hondo and I. Mizuuchi, "Analysis of the 1-joint spring-motor coupling system and optimization criteria focusing on the velocity increasing effect," in *Proc. IEEE Int. Conf. Robot. Automat.*, 2011, pp. 1412–1418.

[14] H. De La Parra and T. Backstrom, "Thermal aspects of field weakening implementation for robotics applications," in *Proc. Eur. Conf. Power Electron. Appl.*, 2005, pp. 6 pp.-P.6. doi: 10.1109/EPE.2005.219766.

[15] W. Roozing, N. Kashiri, and N. G. Tsagarakis, "Enhanced explosive motion for torque controlled actuators through field weakening control," in *Proc. IEEE/RSJ Int. Conf. Intell. Robots Syst.*, 2018, pp. 1–8.

[16] J. Babič, B. Lim, D. Omrčen, J. Lenarčič, and F. C. Park, "A biarticulated robotic leg for jumping movements: Theory and experiments," *J. Mechanisms Robot.*, vol. 1, no. 1, 2009.

[17] R. Niiyama, A. Nagakubo, and Y. Kuniyoshi, "Mowgli: A bipedal jumping and landing robot with an artificial musculoskeletal system," in *Proc. IEEE Int. Conf. Robots Automat.*, 2007, pp. 2546–2551.

[18] K. Radkhah, T. Lens, A. Seyfarth, and O. von Stryk, "On the influence of elastic actuation and monoarticular structures in biologically inspired bipedal robots," in *Proc. EEE RAS-EMBS Int. Conf. Biomed. Robot. Biomechatronics*, 2010, pp. 389–394.

[19] K. Hosoda, Y. Sakaguchi, H. Takayama, and T. Takuma, "Pneumatic-driven jumping robot with anthropomorphic muscular skeleton structure," *Auton. Robots*, vol. 28, no. 3, pp. 307–316, 2010.

[20] Z. Ren, W. Roozing, and N. G. Tsagarakis, "The eleg: A. novel efficient leg prototype powered by adjustable parallel compliant actuation principles," in *Proc. IEEE-RAS 18th Int. Conf. Humanoid Robots.*, 2018, pp. 1–9.

[21] W. Roozing, Z. Ren, and N. G. Tsagarakis, "Design of a novel 3-DoF leg with series and parallel compliant actuation for energy efficient articulated robots," in *Proc. IEEE Int. Conf. Robot. Automat.*, Brisbane, May 2018, pp. 1–8.

[22] "Alberobotics, actuators infosheet," Accessed: Jun. 6, 2020. [Online]. Available: https://alberobotics.it/actuators-data-sheet/file

[23] R. Krishnan, *Permanent Magnet Synchronous and Brushless DC Motor Drives*, 1st ed. Boca Raton, FL, USA: CRC Press, Dec. 2017.

[24] R. Djajadiningrat, W. Roozing, and N. G. Tsagarakis, "Explosive motions with compliant actuation arrangements in articulated robots," in *Proc. 7th IEEE Int. Conf. Biomed. Robot. Biomechatronics*, 2018, pp. 1309–1314.